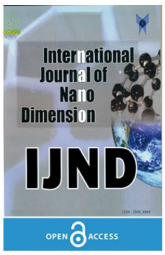

Volume 15, Issue 2, 152415 (1-6)

International Journal of Nano Dimension (IJND)

https://dx.doi.org/10.57647/j.ijnd.2024.1502.15

A comprehensive investigation on electronic properties for quantum-confined Cobalt doped SiC nanotube: a DFT approach

Debarati Dey Roy[1]*, Vusala Nabi Jafarova[2], Aynura Alisa Hadiyeva[2], Pradipta Roy[3]

[1]*Deptartment of Electronics & Communication Engineering, B. P. Poddar Institute of Management & Technology, West Bengal, India.*
[2]*Azerbaijan State Oil and Industry University, Baku, Azerbaijan.*
[3]*Department of Computer Application, Dr. B. C. Roy Academy of Professional Courses, West Bengal, India.*

***Corresponding author:** debaratidey24@gmail.com

RESEARCH PAPER

Received:
14 January 2024
Revised:
27 February 2024
Accepted:
01 March 2024
Published online:
30 March 2024

Abstract:

The investigation of the thermoelectric characterization of magnetic material doped Silicon Carbide (SiC) nanotube (NT) is a challenging aspect for the researchers. Thanks to the Density Functional Theory (DFT) based formalisms help to provide accurate electronic characterization for the nanoscale 2-D models. The investigation of the Device Density of States (DDOS) of the magnetically doped SiC NT is based on the prediction of molecular and atomic level data set. Spin polarization effect is observed for this doped single wall (6,0) chiral type SiC NT. The energy band gap is lower for doped quantum-confined structure (0.98 eV) compared to bulk structure (3.3 eV). The spin density approximation is based on the Hubbard U method. The observed magnetic moment for the doped structure is equal to 1.9 μB. Comparing between anti-ferromagnetic and ferromagnetic stages, the ferromagnetic stage is observed as a more stable phase.

Keywords: DFT; First principle; Co doped SiC; Quantum-confinement

1. Introduction

Thermoelectric characterization for nanoscale 2-D structure is studied and investigated for doped Graphene Nanoribbons (GNR). Boron (B), Nitrogen (N), Silicon (Si), and Beryllium (Be) are the dopant atoms for the GNR [1]. Design descriptors are required to represent fixed-length DDOS that comprises variable energy points [2–5]. Electronic and optical properties of the transition metal doped WS_2 monolayer are changed visibly while DFT is applied for calculation purposes [6]. Structural and physical properties are investigated for the armchair-type nanoribbon $MoSi_2N_4$ while doped with 3-D transition metal. Spintronic properties are also investigated for this nanoribbon [7]. Synthesized ternary nanostructures are to be composed with Cerium (Ce) Chitosan (CS) and TiO_2 quantum dots for the coprecipitation procedure. Depending on the doping concentrations the electronic and physical properties are changed [8]. Ce and Sm along with Co-doped TiO_2 nanomaterials are used to enhance the photocatalytic activities of Rhodamine B dye. Therefore, it is emphasized that the electrochemical characteristics are enhanced due to the doping effect [9]. Graphene is a widely used and accepted nanomaterial. The influence of metal doping increases its activity rigorously [10]. Doping is an important procedure in the semiconductor industry. Not only conventional doping but also the electrical doping process is playing an important role in improving the electronic properties of the nanostructure. Instead of incorporating of foreign molecules, electrical doping makes the electro potential drops between the two ends of the nanoscale devices. This process reduces the chances of contamination due to the external dopants [11–15]. Using

Table 1. A comparative analysis of the proposed work with the existing approaches.

features	references					
	[22]	[23]	[24]	[25]	[26]	proposed work
method	DFT+NEGF	DFT	DFT	DFT+NEGF	DFT+NEGF	DFT
material	mono layer GeS	GNR	ZnO-based nano-fibers	zigzag Phosphorene nanoribbons	GNR	SiC NT
doping agents	N, P, As	Mn	Ag, ZrO_2	V	Ph	Co
width	NR	NR	NR	6 folds	8-order magnitude	2.2nm
length	NR	NR	NR	NR	NR	2.5nm
stress	NR	NR	NR	NR	NR	0.001 eV/$Å^3$
force	NR	NR	NR	0.01 eV/$Å$.	NR	0.001 eV/$Å$

NR=Not reported.

the external doping process the quantum ballistic transmission is improved for these quantum-confined nanostructures. DFT formalisms encourage researchers to investigate the changes during the doping process for this nanoscale structure [16–20]. The natural population analysis which based on strong particle can be played an important role in the molecular stabilization energy [21]. This paper presents the changes of DDOS of the SiC NT while doped with magnetic dopants. The comparison table shows the novelty of the proposed work in Table 1 [22–26].

2. Computational method

This paper has been presented the quantum-confined theoretical model of Cobalt (Co) doped SiC NT. This DFT-based approach is analytically investigated using Atomistix Tool Kit (Quantum -ATK) version 13.8.0. The electronic characterization of this quantum-confined model is based on Local Density Approximation (LDA) and Local Spin Density Approximation (LSDA) methods also. The interactions held between the ions and electrons, and exchange correlation were described by the Fritz-Haber-Institute ion pseudopotentials method and the Perdew Zunger (PZ) functional, respectively. The cut-off kinetic energy is 75 Hartree for this bulk nanostructure. The primitive cell of SiC wurtzite is formatted with 2 Si and 2 C atoms and k-point sampling is performed with $1\times1\times10$ for doped NT. The electronic temperature is kept at 300K. The diluted magnetic nanotubes and cations (Si) are replaced arbitrarily by Co↑x/2 and Co↓x/2 which are magnetic ions. The ↑ and ↓ signs refer to the spintronic direction of the local moment of the impurity magnetic dopants. The simulation parameters for the DFT based analytical model are shown in Table 2.

3. Results and discussion

In this theoretical work, the DFT+LDA method along with Hubbard U analytical corrections (for Si 4d states U=5 eV and for C 2p states U=4.8 eV) have been made. To study the Dilute Magnetic Semiconductor (DMS) devices, transition metals like V, Cr, Co, Fe, Mn, and Ni play a crucial role. The electronic properties of puree Sic NT and Co-doped SiC NT with chiral vector (6, 0) are illustrated with the help of DFT approach. The analytical model of single walled SiC NT (SWSiCNT) is designed whose band gap varies from 0.9 to 1.83 eV [27]. The empirical model of pristine SWSiC NT (6, 0) and Co-doped SWSiC NT are shown in Fig. 1(a) and Fig. 1(b) respectively.
The spintronic view of these two conditions is shown in Fig. 2. The magnetic moments for the Co-doped SiCNT

Table 2. Results of proposed current mirror and comparison with existing designs.

parameters	**value**	**details**
configuration	(A, B, C)	the SiC NT structure along (X, Y, Z) axes
electrodes' Fermi level	0eV	the left and right electrodes' Fermi level lies at 0eV
force tolerance	0.01eV/$Å$	when minimum then sustainability increase
poisson Equation Solver	multi-grid	algorithm used
maximum interaction range between electron orbitals	1 nm	numerical accuracy parameters
no. of steps for iteration	100	increasing steps increasing accuracy
step size	0.25 nm	step size increasing the time of simulation
electron temperature	300K	room temperature operation

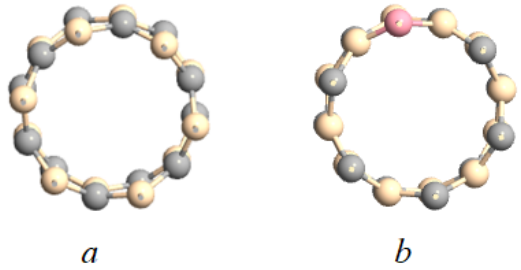

Figure 1. Structure of (a) SiC (6,0) nanotube (silicon-beige, carbon-gray), (b) Si(Co)C (6,0) nanotube (silicon-beige, carbon-gray, cobalt-pink).

structure are shown with 'green' arrows. The magnetic moments are opposite for Si and C atoms and therefore, SiC are neutral with respect to the magnetic moments. Whereas, incorporation of Co atom induced the magnetic moment to the SiCNT.

The half-metallic property of the SWSiCNT is raised due to the ferro magnetic dopant Co. Total DDOS (TDDOS) of SWSiCNT and SWSi(Co)C-NT are investigated using DFT formalisms. The 2D figures of pristine and Co-doped SiC nanotubes using DFT based approach are shown in Fig. 3(a) and Fig. 3(b), respectively.

The results obtained for pristine SWSiCNT (8, 0) using DFT-GGA method and the band gap is 1.05 which is reported for this system [28]. For pure SWSiCNT (5, 0) shows metallic conductivity [29]. Totally different TDDOS are obtained for pristine and Co doped SiCNT which are shown in Fig. 3(a) and 3(b) respectively. Spin-up and spin-down conditions are reflected in the graphs using DFT-LSDA-based calculations. Near Fermi energy level 0 eV higher values of TDDOS are observed for both pure and doped SWSiCNT. In higher energy level the TDDOS are observed with lower concentration.

From DFT-LSDA+U calculations we obtained that the chiral vector for SWSiCNT has a direct band gap ($\Gamma - \Gamma$) and the wide of the band gap is 0.98 eV for undoped SWSiC nonmagnetic NT and this result is observed to be smaller than that of the pristine SiCNT. This fact is closer to the result in [28, 30]. It was studied the influence of the structure

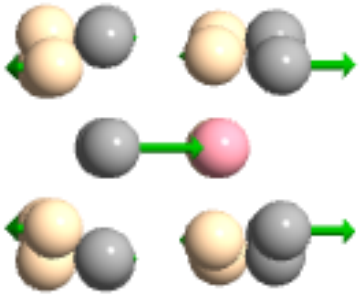

Figure 2. Spin-polarization view for Co-doped SiCNT: Si-beige, C-gray, Co-pink. Magnetic moments are shown by green arrows.

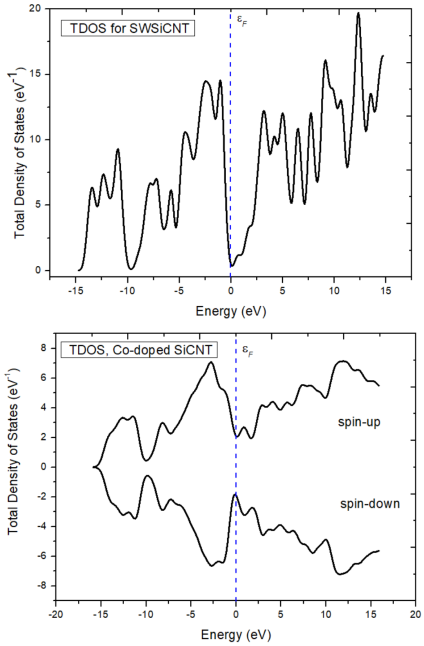

Figure 3. Spin-polarized TDDOS model for (a) SWSiCNT and, (b) SWSi(Co)C-NT.

for the magnetic doping SiC film and obtained that Co-doped film exhibit intrinsic ferromagnetism at 300 K [31]. From the first principles simulations, results are obtained for undoped SWSiC is shown in Fig. 4(a) and spin-polarized band structures for spin-up and spin-down states which are

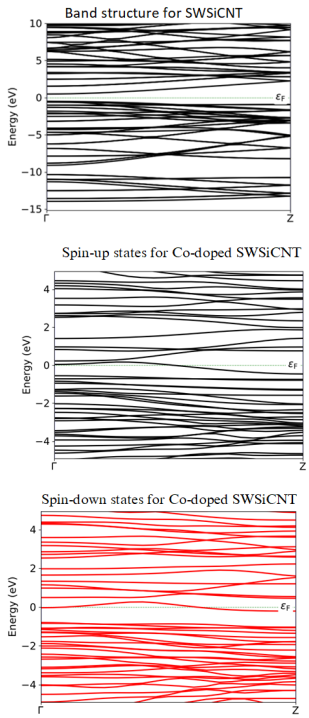

Figure 4. Electronic band structure for undoped, (a) SWSiC (6,0) nanotube (Eg=0.98 eV), (b) Co-doped (6,0) single wall SiCNT (Spin-up), (c) Co-doped (6,0) single wall SiCNT (Spin-down).

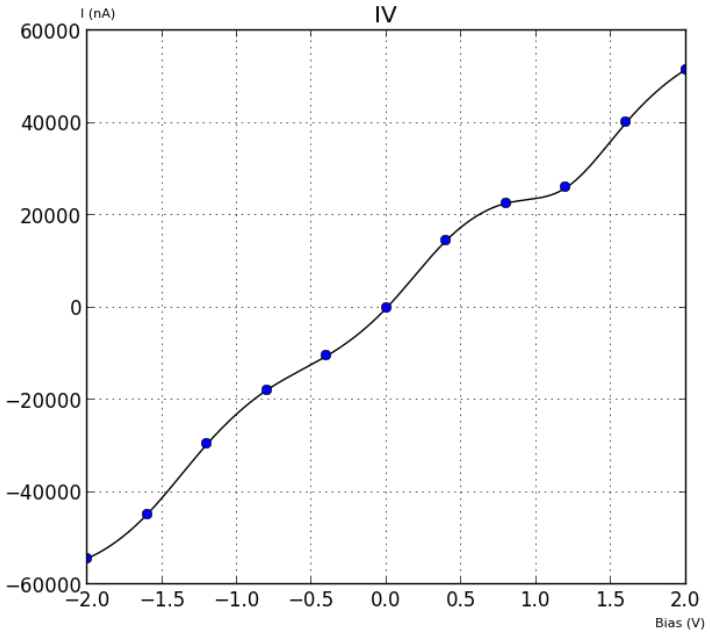

Figure 5. IV characteristics of the Co doped SiCNT.

shown in Fig. 4(b) and Fig. 4(c). The multilayer perception (MLP) model is used to map these illustrations in the form of matrix representation in real-space linear combination of atomic orbitals (LCAO) Hamiltonian [31, 32]. From the first-principles simulations the total magnetic moment of single and double Co^{+2} - doped SiCNT systems are 1.896 and 5.2 μB, respectively. This fact due to the double exchange because of *pd* orbital hybridization between impurity Co 3*d*- and host C 2*p*-states. The carbon *p*-orbitals play significant roles in the stability of Ferro-magnetic (FM) phase. Main contribution of this doping is to magnetize of nanotube from 3 C atoms ($\sim$3.26 μB) is chemically bonded with Co impurity atom. The negligible negative contribution has removed for the purpose of magnetization from impurity atom ($\sim$0.16 μB). From the total energy calculations for FM (E_{FM}=-5479.56293 eV) and anti-ferro magnetic (AFM) (E_{FM}=-5479.61682 eV) phases the energy difference ($\Delta E = E_{AFM} - E_{FM}$) indicating that the AFM state more stable than FM state for Co : SiCNT.

The current-voltage (IV) characteristics of the proposed model have been shown in Fig. 5. This graph shows that the satisfactory current flows through the SiCNT after doping with Co. This emphasis that Co atoms increase the numbers of charge carriers through the central molecular region of the Co : SiCNT model. The crosstie-tick Table 3 shows the novelty and comparative analysis of the proposed work with the existing works.

4. Conclusion

The half-metallic character of SWSiCNT was discovered through investigation with and without co-doping. The result of co-doping is an improvement in the metallic property. This half-metallic character is induced in the SiCNT because of the ferromagnetic property of the Co atoms. This quantum-confined nanostructure's metallic nature can be determined with the aid of DFT-based formalisms. Since TDDOS concentrations are larger close to the Fermi energy level (0 eV), the structure's stability was disclosed by the TDDOS nature. The energy gap for the FM and AFM further demonstrates the SWSiC(Co)NT's thermodynamic stability. It follows that this structure has demonstrated its importance as a raw material for electronic applications of the future.

Table 3. Cross-tick table for novelty and comparative analysis.

features	**references**					
	[22]	[23]	[24]	[25]	[26]	Proposed work
DFT	√	√	√	√	√	√
multilayer	×	√	√	√	√	√
doping	√	√	√	√	√	√
low stress	×	×	×	×	×	√
lower force	×	×	×	√	NR	√

Ethical Approval
This manuscript does not report on or involve the use of any animal or human data or tissue. So the ethical approval does not applicable.

Funding
No funding was received to assist with conducting this study and the preparation of this manuscript.

Authors Contributions
All authors have contributed equally to prepare the paper.

Availability of Data and Materials
The data that support the findings of this study are available from the corresponding author upon reasonable request.

Conflict of Interests
The authors declare that they have no known competing financial interests or personal relationships that could have appeared to influence the work reported in this paper.

References

[1] S.Y. He, H.L. Shi, J. Yang, Y.H. Ren, Q.Z. Han, L.J. Gong, and Z.T. Jiang. A comparative investigation into the thermoelectric properties of doped graphene nanoribbons in different doping manners. *Diam. Relat. Mater*, **135**:109889, 2023. DOI: https://doi.org/10.1016/j.diamond.2023.109889.

[2] A. Seko, H. Hayashi, K. Nakayama, A. Takahashi, and I. Tanaka. Representation of compounds for machine-learning prediction of physical properties. *Phys. Rev. B*, **95**:144110, 2017. DOI: https://doi.org/10.1103/PhysRevB.95.144110.

[3] D. Xue, P.V. Balachandran, J. Hogden, J. Theiler, D. Xue, and T. Lookman. Accelerated search for materials with targeted properties by adaptive design. *Nat. Commun*, **7**:11241–11246, 2016. DOI: https://doi.org/10.1038/ncomms11241.

[4] L.M. Ghiringhelli, J. Vybiral, S.V. Levchenko, C. Draxl, and M. Scheffler. Big data of materials science: Critical role of the descriptor. *Phys Rev Lett*, **114**:105503, 2015. DOI: https://doi.org/10.1103/PhysRevLett.114.105503.

[5] O.A. Von Lilienfeld, R. Ramakrishnan, M. Rupp, and A. Knoll. Fourier series of atomic radial distribution functions: A molecular fingerprint for machine learning models of quantum chemical properties. *Int. J. Quant. Chem*, **115**:1084–1093, 2015. DOI: https://doi.org/10.1002/qua.24912.

[6] S. Chowdhury, P. Venkateswaran, and D. Somvanshi. Biaxial strain-modulated electronic and optical properties of transition metals doped-WSe_2 monolayer. *Phys. B: Condens. Matter*, **653**:414668, 2023. DOI: https://doi.org/10.1016/j.physb.2023.414668.

[7] X.Q. Su and X.F. Wang. Electronic and spintronic properties of armchair $MoSi_2N_4$ nanoribbons doped by 3D transition metals. *Nanomater.*, **13**:676–681, 2023. DOI: https://doi.org/10.3390/nano13040676.

[8] M. Ikram, R. Raees, A. Haider, A. Ul-Hamid, J. Haider, I. Shahzadi, W. Nabgan, S. Goumri-Said, M.B. Kanoun, and S. Ali. Enhanced photocatalytic and antibacterial activity of TiO_2 quantum dots doped with Cerium/Chitosan for environmental remediation: Experimental and theoretical approaches. *Mater. Chem. Phys*, **297**:127462, 2023. DOI: https://doi.org/10.1016/j.matchemphys.2023.127462.

[9] Y. Slimani, M.A. Almessiere, M.J. Mohamed, E. Hannachi, S. Caliskan, S. Akhtar, A. Baykal, and M.A. Gondal. Synthesis of Ce and Sm Co-Doped TiO_2 nanoparticles with enhanced photocatalytic activity for rhodamine B dye degradation. *Catalys*, **13**:668–673, 2023. DOI: https://doi.org/10.3390/catal13040668.

[10] Ö. Ünlü and İ.A. Morkan. A computational study: Structural and electronic properties of some transition metal doped bilayer graphene systems. *Int. J. Innovat. Approach. Sci. Res*, **6**:34–45, 2022. DOI: https://doi.org/10.29329/ijiasr.2022.454.2.

[11] D.D. Roy, M. Chanda, and D. De. Spin transport properties in DNA & electrically doped iron QD organo-metallic junction. *Mater. Today: Proceed*, **71**:165–173, 2022. DOI: https://doi.org/10.1016/j.matpr.2022.08.332.

[12] D. Dey Roy, P. Roy, and D. De. Biomolecular nano scale devices using first principle paradigm: A comprehensive survey. *Int. J. Nano Dimens*, **14**:115–125, 2023. DOI: https://doi.org/10.22034/ijnd.2023.1980309.2206.

[13] P. Roy, D. Dey, and D. De. Computational investigation of quantum transport to design single-strand DNA logic gate using silicon carbide nanotube electrode. *IETE J. Res*, **68**:299–307, 2022. DOI: https://doi.org/10.1080/03772063.2019.1604171.

[14] D.D. Roy, P. Roy, M. Chanda, and D. De. Ultra-low voltage adenine based gas sensor to detect H_2 and NH_3 at room temperature: First-principles paradigm. *Int. J. Hydrogen Energy*, **48**:4931–4941, 2023. DOI: https://doi.org/10.1016/j.ijhydene.2022.11.040.

[15] D.D. Roy and D. De. Predicting model of I–V characteristics of quantum-confined GaAs nanotube: A machine learning and DFT-based combined framework. *J. Comput. Electron*, **22**:999–1009, 2023. DOI: https://doi.org/10.1007/s10825-023-02056-2.

[16] S. Saini and S. Choudhary. A DFT study of transition metal doped two-dimensional bismuth (bismuthene) for spintronics applications. *Adv. Nat. Sci: Nanosc. Nanotechnol*, **13**:53–58, 2022. DOI: https://doi.org/10.1088/2043-6262/ac53fe.

[17] C. Guo, J. Li, and T. Wang. A theoretical study on adjustment of negative differential resistance effect in monolayer GeS via substitutional doping. *Phys. Status Solidi (B)*, **260**:2200499, 2023. DOI: https://doi.org/10.1002/pssb.202200499.

[18] N. Nasir, M.H. Rashid, S.A. Cheema, A. Rasheed, N. Sabir, Z. Tanveer, T. Hassan, and Q. Anjam. An experimental and simulation evaluation of the structural, morphological and optical characters of ZnO-based nano-fibers doped with Ag and ZrO_2. *Optik.*, **265**:169383, 2022. DOI: https://doi.org/10.1016/j.ijleo.2022.169383.

[19] R. Sharma, N. Kaur, B.C. Choudhary, and J.K. Goswamy. DFT based study of transition metals (Au, Ag, Pd & Pt) doped graphitic carbon nitride (gCN) monolayer as a CO gas sensor. *Phys. Scripta*, **97**: 065706, 2022. DOI: https://doi.org/10.1088/1402-4896/ac6e98.

[20] H.H. Zhu, N. Liu, Y.L. Feng, K.L. Yao, and S.Y. Wang. Dual spin filtering and negative differential resistance effects in vanadium doped zigzag phosphorene nanoribbons with different edge passivations. *AIP Adv*, **12**:75687, 2022. DOI: https://doi.org/10.1063/5.0075687.

[21] M.S. Sadjadi, B. Sadeghi, and K. Zare. Natural bond orbital (NBO) population analysis of cyclic thionylphosphazenes, [NSOX $(NPCl_2)_2$]; X= F (1), X= Cl (2). *J. Molec. Struc: THEOCHEM*, **817**:27–33, 2007. DOI: https://doi.org/10.1016/j.theochem.2007.04.015.

[22] D. Dey, P. Ro, and D. De. Atomic scale modeling of electrically doped pin FET from adenine based single wall nanotube. *J. Molec. Graph. Modell*, **76**:118–127, 2017. DOI: https://doi.org/10.1016/j.jmgm.2017.06.024.

[23] R. Jyoti, R. Kashyap, M. Chauhan, B.C. Choudhary, A. Kumar, and R.K. Sharma. Adsorption study of pristine and manganese doped graphene nanoribbon for effective methane gas sensing-A DFT study. *Phys. B: Condens. Matter*, **644**:414212, 2022. DOI: https://doi.org/10.1016/j.physb.2022.414212.

[24] D. Dey, P. Roy, and D. De. Electronic transport properties of electrically doped cytosine based optical molecular switch with single-wall carbon nanotube electrodes. *IET Nanobiotechnol*, **13**:484–492, 2019. DOI: https://doi.org/10.1049/iet-nbt.2018.5375.

[25] D. Dey, P. Roy, and D. De. First principle study of the self-switching characteristics of the guanine based single optical molecular switch using carbon nanotube electrodes. *IET Nanobiotechnol*, **13**:237–241, 2019. DOI: https://doi.org/10.1049/iet-nbt.2018.5227.

[26] V.T. Phuc, P.T.B. Thao, R. Ahuja, and N.T. Tien. Effect of phosphorus doping positions on electronic transport properties in the sawtooth penta-graphene nanoribbon: First-principles insights. *Solid State Communic*, **353**:114859, 2022. DOI: https://doi.org/10.1016/j.ssc.2022.114859.

[27] M. Zhao, Y. Xia, F. Li, R.Q. Zhang, and S.T. Lee. Strain energy and electronic structures of silicon carbide nanotubes: Density functional calculation. *Phys. Rev. B*, **71**:085312, 2005. DOI: https://doi.org/10.1103/PhysRevB.71.085312.

[28] A.T. Mulatu, K.N. Nigussa, and L.D. Daja. Structural and electronic properties of zigzag single wall (8, 0),(9, 0), and (10, 0) silicon carbide nanotubes. *Materialia*, **20**:101257, 2021. DOI: https://doi.org/10.1016/j.mtla.2021.101257.

[29] E.V. Larina, V.I. Chmyrev, V.M. Skorikov, P.N. D'yachkov, and D.V. Makaev. Band Structure of silicon carbide nanotubes. *Inorg. Mater*, **44**:823–834, 2008. DOI: https://doi.org/10.1134/S0020168508080086.

[30] M. Methfessel and A. Paxton. High-precision sampling for Brillouin-zone integration in metals. *Phys. Rev. B*, **40**:3616–3621, 1989. DOI: https://doi.org/10.1103/PhysRevB.40.3616.

[31] X.K. Sun, J.W. Liu, K.L. Liu, S.H. Wang, L.L. Zhao, W. Qin, G.L. Wang, M. Meng, J.T. Li, and X. Dong. Effect of temperature on the structure and magnetic properties of Co doped SiC films. *Superlatt. Microstruc*, **107**:144–149, 2017. DOI: https://doi.org/10.1016/j.spmi.2017.04.024.

[32] J.C. Slater and G.F. Koster. Simplified LCAO method for the periodic potential problem. *Phys. Rev*, **94**:1498–1524, 1954. DOI: https://doi.org/10.1103/PhysRev.94.1498.